
SHORTCUT-CONNECTED EXPERT PARALLELISM FOR ACCELERATING MIXTURE OF EXPERTS

Weilin Cai¹ Juyong Jiang¹ Le Qin¹ Junwei Cui¹ Sunghun Kim¹ Jiayi Huang^{1*}

ABSTRACT

Expert parallelism has been introduced as a strategy to distribute the computational workload of sparsely-gated mixture-of-experts (MoE) models across multiple computing devices, facilitating the execution of these increasingly large-scale models. However, the *All-to-All communication* intrinsic to expert parallelism constitutes a significant overhead, diminishing the MoE models’ efficiency. Current optimization approaches offer some relief, yet they are constrained by the sequential interdependence of communication and computation operations. To address this limitation, we present a novel shortcut-connected MoE (ScMoE) architecture with an overlapping parallel strategy, which effectively decouples communication from its conventional sequence, allowing for a substantial overlap of 70% to 100% with computation. When compared with the prevalent top-2 MoE architecture, ScMoE demonstrates training speed improvements of 30% and 11%, and inference improvements of 40% and 15%, in our distributed environments with PCIe and NVLink hardware, respectively, where communication constitutes 60% and 15% of the total MoE time consumption. Building on the ScMoE architecture, we further implement an expert offloading strategy to facilitate memory-limited inference, optimizing latency through the overlap of expert migration. Additionally, extensive experiments and theoretical analyses indicate that ScMoE not only achieves comparable but in some instances surpasses the model quality of existing approaches.

1 INTRODUCTION

In recent years, Transformer-based large language models (LLMs) have significantly propelled the fields of Natural Language Processing (Vaswani et al., 2017; Brown et al., 2020; Wei et al., 2022b; Ouyang et al., 2022; Wei et al., 2022a; Chowdhery et al., 2023; Achiam et al., 2023), Computer Vision (Dosovitskiy et al., 2021; Liu et al., 2021), and Multimodality (Lu et al., 2019; Zhou et al., 2022; Zhang et al., 2021; Zhu et al., 2023). The sparsely-gated mixture-of-experts (MoE) approach has been integral in increasing parameter counts and enhancing model performance across various modalities (Shazeer et al., 2017; Riquelme et al., 2021; Mustafa et al., 2022; Jiang et al., 2024). Expert parallelism (Lepikhin et al., 2021; Fedus et al., 2022) has emerged as a viable strategy to distribute MoE computations efficiently over multiple devices, synergizing with conventional parallelism techniques (Hwang et al., 2022; Singh et al., 2023) such as data parallelism (Rajbhandari et al., 2020; 2021) and model parallelism (Narayanan et al., 2021; Smith et al., 2022).

Nevertheless, expert parallelism incurs substantial *All-to-All communication* overhead (Lepikhin et al., 2021; Fedus et al., 2022), which can contribute to approximately 50% of the total time in intra-node multi-GPUs or multi-nodes distributed environments (see Figure 1), thus forming a critical bottleneck in scaling MoE models (Nie et al., 2022; Hwang et al., 2022; Mayer & Jacobsen, 2020; Smith et al., 2022). Despite existing optimizations such as hierarchical All-to-All (He et al., 2022; Nie et al., 2022) and pipelining (Hwang et al., 2022; Zhang et al., 2023) strategies that mitigate communication delays and partially overlap communication with computation, the communication challenge persists due to the inherent sequential dependencies between these operations (Wang et al., 2023). To address this constraint, our intuitive idea is to reconstruct the inputs of MoE layer by incorporating not only the current-layer but also the preceding-layer representations through a shortcut connection, thereby refining the communication dependencies and expanding the potential for optimization.

In this paper, we introduce the shortcut-connected MoE (ScMoE) architecture, which completely decouples communication processes from the sequence of conventional MoE models. Our architecture is built upon the standard top-2 MoE (see Figure 2 (a)) which typically substitutes the Multi-Layer Perceptron (MLP) module with a top-2 gating MoE module in every second Transformer block (refer to

*Corresponding author. ¹The Hong Kong University of Science and Technology (Guangzhou). Correspondence to: Weilin Cai <wcai738@connect.hkust-gz.edu.cn>, Jiayi Huang <hji@hkust-gz.edu.cn>.

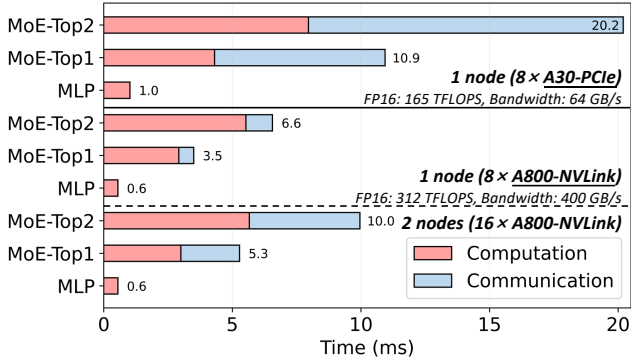


Figure 1. The overhead of MLP and top-2/top-1 MoE in a transformer block of SwinV2-MoE-S (Hwang et al., 2022) model, allocating one expert per GPU with expert parallelism. The All-to-All communication takes up 60% of total time on a single node with 8x A30 GPUs, but drops to 15% on 8x A800 due to the latter’s 6x higher bandwidth provided by GPU-to-GPU NVLink (Foley & Danskin, 2017). Despite benefiting from NVLink, communication still approaches 50% due to the lower-bandwidth inter-node Ethernet (Li et al., 2020) when scaling across multiple nodes.

the Transformer block with MoE module as “current layer”, and the preceding one without MoE module as “preceding layer”). Diverging from the top-2 approach, our ScMoE utilizes a top-1 MoE module to process preceding-layer representations via a shortcut connection, while employing a shared expert (an MLP module) to process current-layer representations. These two processes are independently managed in parallel, with their results integrated into the final output of the current layer. Furthermore, we select the intermediate representations between the Attention and MLP modules in the preceding layer as the input for the top-1 MoE. Our experiments on various preceding-layer representations (output, intermediate, input) indicate that this choice achieves optimal accuracy and a relatively longer overlap duration.

To efficiently overlap the decoupled communication and computation within our ScMoE architecture, we implement an adaptive overlapping parallel strategy that dynamically schedules operators based on actual performance metrics. Relative to existing optimization strategies, our approach not only doubles the overlap duration compared to the pipelining (Huang et al., 2019; Hwang et al., 2022) but also realizes complete overlapping of communication in scenarios where communication time does not surpass the computation duration. Furthermore, our method essentially advances the MoE architecture in algorithm aspect, which is device-agnostic to improve the efficiency of MoE model, thus ensuring a broad applicability across various hardware configurations and maintaining compatibility with current optimizations.

Additionally, existing studies (Hwang et al., 2023b; Yi et al., 2023) offload expert parameters to CPU memory in memory-limited inference scenarios where GPU cannot store the full

MoE model. These studies utilize information in preceding layers to predict expert selection for the current MoE layer, enabling early expert migration from CPU to GPU and overlapping it with model computation. In contrast to existing speculative expert migration methods, we implement an expert offloading strategy with overlapping determinate migration, built upon our ScMoE that inherently advances expert selection to the preceding layer.

The extensive experimental results reveal that compared with the standard top-2 MoE, our ScMoE architecture achieves training speed improvements of 30% and 11% in 8x A30-PCIe and 8x A800-NVLink scenarios characterized by high and low communication overheads, respectively, and deliver inference speed improvements of 40% and 15%. Besides, our ScMoE has been demonstrated through experiments and theoretical analysis to attain or exceed the model quality of existing methods in both vision and language downstream tasks. In memory-limited inference, our expert offloading strategy reduces peak GPU memory usage by up to 60% and decreases expert migration costs by up to 75% through overlapping with computation. In addition, we conduct an in-depth analysis of our ScMoE, investigating the proposed shortcut connection and exploring the potential reasons for its algorithmic effectiveness.

In summary, our contributions are as follows:

- We propose the shortcut-connected MoE (ScMoE) architecture that breaks conventional interdependency between communication and computation in distributed MoE models, bypassing the restrictions imposed on current communication optimization techniques.
- We develop an adaptive overlapping strategy for advancing expert parallelism with our shortcut-connected MoE, which significantly improves the efficiency of MoE models and ensures broad compatibility.
- We implement an expert offloading strategy with overlapping determinate expert migration upon our ScMoE, enhancing efficiency in memory-limited inference.
- We conduct empirical evaluation and theoretical analysis on our methods, confirming that our methods accelerate MoE models while achieving comparable or even better model quality compared to existing methods, and offer in-depth analysis and discussion on the effectiveness of the proposed shortcut connection.

2 BACKGROUND & RELATED WORK

2.1 Sparsely-Gated Mixture of Experts

The Sparsely-Gated Mixture-of-Experts (Shazeer et al., 2017) (MoE) layer is composed of multiple Multi-Layer

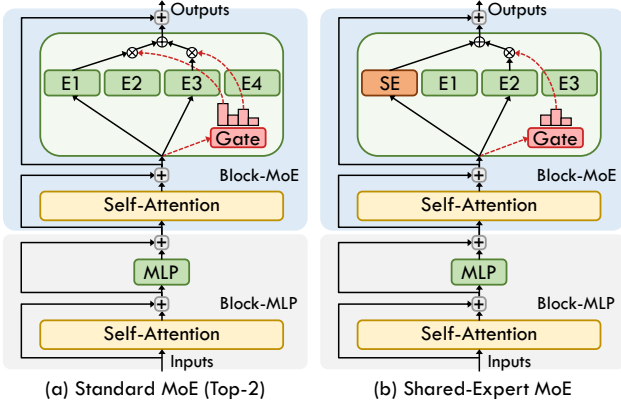


Figure 2. Illustrations of the standard top-2 MoE architecture (a) and the corresponding shared-expert MoE architecture (b). “SE” in (b) denotes the shared expert.

Perceptron (MLP) sub-networks, termed “experts”, and employs a trainable gating network to selectively activate a subset of these experts during each iteration. Given N expert networks $\{E_i\}_1^N$, gating network G and input representation x , the output of MoE module can be written:

$$MoE(x) = \sum_{i=1}^N G(x)_i E_i(x) \quad (1)$$

Following the prevailing approach in existing MoE research, we use the noisy top- k softmax gating network to select k experts for the computation, formalized by

$$G(x) = \text{Softmax}(\overline{\text{TopK}}(H(x), k)) \quad (2)$$

$$\overline{\text{TopK}}(H(x), k)_i = \begin{cases} H(x)_i, & \text{if } H(x)_i \in \text{TopK}(H(x)). \\ -\infty, & \text{otherwise.} \end{cases} \quad (3)$$

$$H(x)_i = (x \cdot W_{gate})_i + \epsilon_i, \quad (4)$$

$$\epsilon_i = \text{StandardNormal}() \cdot \text{Softplus}((x \cdot W_{noise})_i), \quad (5)$$

where ϵ is tunable Gaussian noise, W_{gate} and W_{noise} denote two trainable weight matrices.

Leveraging sparse output of $G(x)$, this approach significantly increases the number of model parameters without causing a proportional increase in computational demand. The value of k can be set to 1 or 2 or even higher values. Opting for a larger k moves the model closer to the dense architecture, which generally results in higher prediction accuracy (Riquelme et al., 2021), but also leads to larger execution overhead.

Figure 2 (a) illustrates the prevailing top-2 MoE architecture. Each Transformer block with MoE module, denoted by a light blue block and referred to as “Block-MoE,” replaces the MLP with a set of experts (“E1, E2, E3, E4”) and a gating network (“Gate”). Following prior work (Lepikhin

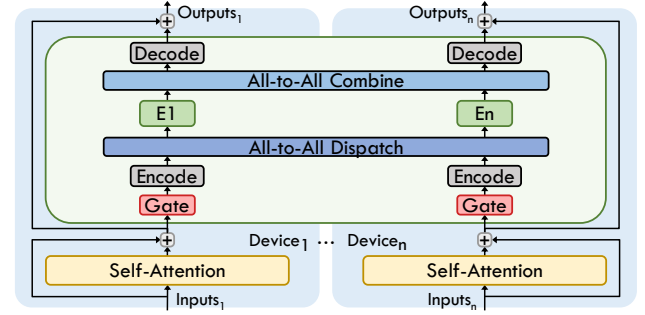


Figure 3. Illustration of scaling MoE transformer layer across multiple devices with expert parallelism.

et al., 2021; Du et al., 2022; Shen et al., 2023; Hwang et al., 2022), the “Block-MoE” is interspersed with the conventional Transformer block, depicted as a gray block and referred to as “Block-MLP.”

Shared Expert. In contrast to the standard top-2 MoE architecture, the shared-expert MoE incorporates a fixed dense MLP module to process all input tokens, combining its output with the result from the top-1 gating expert for each token, as illustrated in Figure 2 (b). Given the shared expert SE , the output of the MoE module is formulated as:

$$MoE(x) = SE(x) + \sum_{i=1}^N G(x)_i E_i(x) \quad (6)$$

This method, initially proposed by DeepSpeed-MoE (Rajbhandari et al., 2022), activates the same number of experts as standard MoE for computation while reducing dynamic expert selection and communication volume. Extensive empirical results from DeepSpeed-MoE and subsequent studies (Dai et al., 2024; Team, 2024) demonstrate that the shared expert achieves on-par or even better model quality, leading to its increasing application (Xue et al., 2024; Wu et al., 2023; Chen et al., 2024; Gou et al., 2023; Gao et al., 2024).

2.2 Expert Parallelism

To facilitate efficient distributed training and inference of MoE models, expert parallelism is proposed to allocate unique experts to each distributed computing device such as GPU and TPU, and map tokens to their corresponding experts through All-to-All communication across the participating devices (Lepikhin et al., 2021; He et al., 2021; Nie et al., 2022). As illustrated in Figure 3, the workflow of MoE employing expert parallelism is segmented into the following sequential operations: gate routing, input encode, All-to-All dispatch, expert computation, All-to-All combine, and output decode. To enhance the efficiency, input encode is employed to aggregate the token data layout to a contiguous format before All-to-All dispatch, and output decode is the inverse process after All-to-All combine. Furthermore, the integration of expert parallelism with other parallelisms

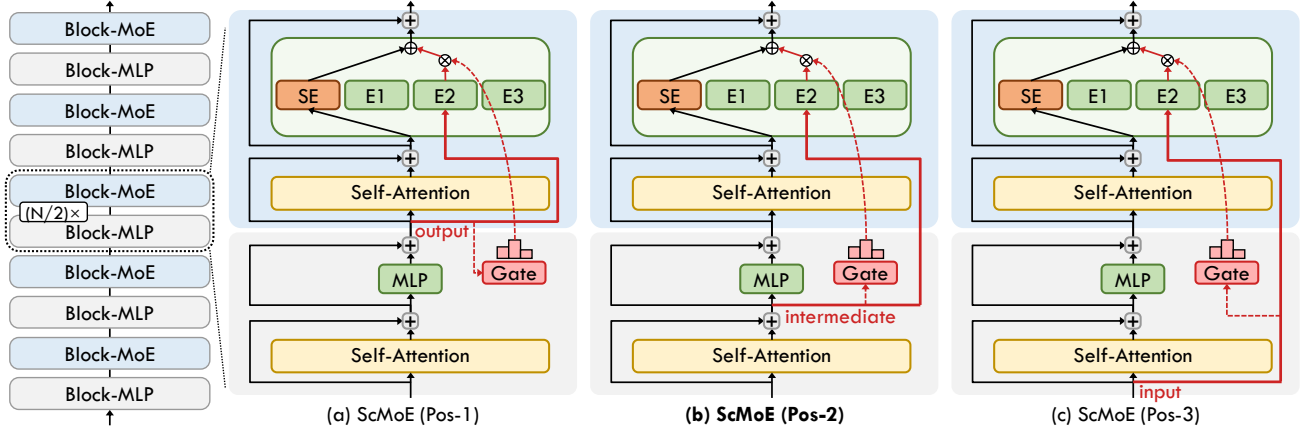


Figure 4. Illustrations of various ScMoE architectures with shortcut connections to different positions of the preceding layer: (a) “Pos-1” output, (b) “Pos-2” intermediate, and (c) “Pos-3” input. The red line indicates the transmission of the preceding-layer representations to the MoE via a shortcut connection. To streamline the explanation, details regarding pre-layer normalization (Pre-Norm) and dropout procedures have been excluded. The ScMoE (Pos-2) configuration (b) is selected as the default ScMoE architecture for further implementations and experiments due to its superior performance, as shown in Table 1.

(Hwang et al., 2022; Singh et al., 2023; Fedus et al., 2022; Zheng et al., 2022) has been explored to support the scaling of larger MoE models on extensive distributed systems.

However, the All-to-All communication used for token transfer has been a primary factor limiting the efficiency of distributed MoE models, as illustrated in Fig 1. To address this issue, we enhance the MoE architecture and expert parallelism with shortcut connections, significantly overlapping communication costs with computation.

2.3 Memory-Limited Inference of MoE Models

While MoE effectively enhances LLMs in terms of model quality, it faces significant deployment challenges during on-device inference due to high memory demand. A common approach is to offload expert parameters to CPU memory (Shen et al., 2022) in scenarios where GPU memory is insufficient to store the entire MoE model. Since the migration of activated expert parameters from CPU to GPU, which occurs after expert selection, blocks expert computation until the transfer is complete, existing studies (Hwang et al., 2023b; Yi et al., 2023; Du et al., 2024) have explored prefetching the experts. For instance, Pre-gated MoE (Hwang et al., 2023b) uses information from preceding layers to predict expert selection, allowing for preloading of expert parameters into GPU memory, as shown in Figure 7. This method enables overlapping the expert migration duration with the computation of preceding modules.

However, speculative expert migrations can suffer from estimation inaccuracies, as they deviate from the original logic of pre-trained models, potentially reducing inference accuracy. In contrast, we enhance the MoE architecture with a shortcut connection, utilizing the MoE module to process preceding-layer representations. This allows us to

Table 1. Test top-1 accuracy and overlap duration of pre-trained SwinV2-MoE-S models with various ScMoE configurations (illustrated in Figure 4). \mathcal{T}_{Atten} , \mathcal{T}_{SE} , and \mathcal{T}_{MLP} represent the durations of Attention, shared expert, and MLP, respectively.

ScMoE	ImageNet-1K (Acc@1 \uparrow)	Overlap Duration
Pos-1	79.14%	$\mathcal{T}_{Atten} + \mathcal{T}_{SE}$
Pos-2	79.38%	$\mathcal{T}_{Atten} + \mathcal{T}_{SE} + \mathcal{T}_{MLP}$
Pos-3	79.20%	$2\mathcal{T}_{Atten} + \mathcal{T}_{SE} + \mathcal{T}_{MLP}$

implement an expert offloading strategy with overlapping determinate migration, maintaining the pre-trained logic.

3 SHORTCUT-CONNECTED MOE DESIGNS

In the prevailing Transformer-based model, the MoE module substitutes MLP to sequentially manipulate intermediate representations (Lepikhin et al., 2021; Du et al., 2022; Shen et al., 2023), impeding the efficacy of existing optimization strategies (He et al., 2022; Nie et al., 2022; Hwang et al., 2022; Zhang et al., 2023) due to the limited interaction within the MoE module. To address the aforementioned limitations, we propose the shortcut-connected MoE (ScMoE) architecture (Section 3.1), which enables optimization opportunities for computation-communication overlap for expert parallelism (Section 3.2) and determinate expert migration for memory-limited inference (Section 3.3).

3.1 Architectural Design

In this section, we introduce the shortcut-connected MoE (ScMoE) architecture. Unlike prevailing MoE architectures, illustrated in Figure 2, which focus on processing intermediate representations within the current layer (the Transformer block containing the MoE), our ScMoE processes

representations from both the current and preceding layers. Specifically, ScMoE employs a top-1 MoE module to handle representations from the preceding layer via a shortcut connection, while a shared expert processes the current-layer representations. These two operations are conducted independently, with their outcomes integrated into the final output of the current layer, facilitating communication and computation overlap between these two processes.

While the shared expert processes the same intermediate representations in the current layer as the prevailing MoE approaches, we explore three distinct preceding-layer representations for ScMoE’s top-1 MoE process, as illustrated in Figure 4. The configurations “Pos-1” (a), “Pos-2” (b), and “Pos-3” (c) represent shortcuts connecting different positions of the preceding layer: output, intermediate, and input, respectively.

Based on our experimental results presented in Table 1, the configuration “Pos-2,” which selects intermediate representations between the Attention and MLP modules in the preceding layer as input for the top-1 MoE module, achieves optimal accuracy (79.38%) and the second longest overlap duration ($\mathcal{T}_{Atten} + \mathcal{T}_{SE} + \mathcal{T}_{MLP}$). Consequently, we have chosen ScMoE (Pos-2) as the default ScMoE architecture for subsequent implementations and experiments. This ScMoE architecture can be formulated as follows:

Block-MoE:

$$\mathcal{H}_{l+1}^{\text{ScMoE}} = \mathcal{H}_{l+1}^{\text{MH}} + SE^{(l+1)}(\mathcal{H}_{l+1}^{\text{MH}}) + \sum_{i=1}^N G(\mathcal{H}_i^{\text{MH}})_i E_i(\mathcal{H}_i^{\text{MH}}) \quad (7)$$

$$\mathcal{H}_{l+1}^{\text{MH}} = \mathcal{H}_i^{\text{MLP}} + \text{MultiHead}_{\text{MoE}}^{(l+1)}(\mathcal{H}_i^{\text{MLP}}) \quad (8)$$

Block-MLP:

$$\mathcal{H}_i^{\text{MLP}} = \mathcal{H}_i^{\text{MH}} + \text{MLP}^{(l)}(\mathcal{H}_i^{\text{MH}}) \quad (9)$$

$$\mathcal{H}_i^{\text{MH}} = \mathcal{H}_{l-1} + \text{MultiHead}_{\text{MLP}}^{(l)}(\mathcal{H}_{l-1}) \quad (10)$$

where $\mathcal{H}_{l+1}^{\text{ScMoE}}$ refers to the output from the MoE sub-layer, $\mathcal{H}_{l+1}^{\text{MH}}$ signifies the output from the Multi-Head Attention (MultiHead) sub-layer $\text{MultiHead}_{\text{MoE}}^{(l+1)}(\cdot)$ in the $(l+1)$ -th Transformer block (“Block-MoE”). $SE^{(l+1)}(\cdot)$ denotes the shared expert while E_1, \dots, E_n represent the N gate-selected experts. The gating network $G(\cdot)$ is referred to as Equation 2. $\mathcal{H}_i^{\text{MLP}}$ and $\mathcal{H}_i^{\text{MH}}$ are the outputs of the MLP sub-layer $\text{MLP}^{(l)}(\cdot)$ and the MultiHead sub-layer $\text{MultiHead}_{\text{MLP}}^{(l)}(\cdot)$, respectively, in the l -th Transformer block (“Block-MLP”). Note that we omit the pre-layer normalization and dropout for simplicity.

In addition, we provide an in-depth theoretical analysis of our proposed ScMoE architecture in Appendix A.1, elucidating the propagation of gradients to guarantee consistent training and preserve model quality.

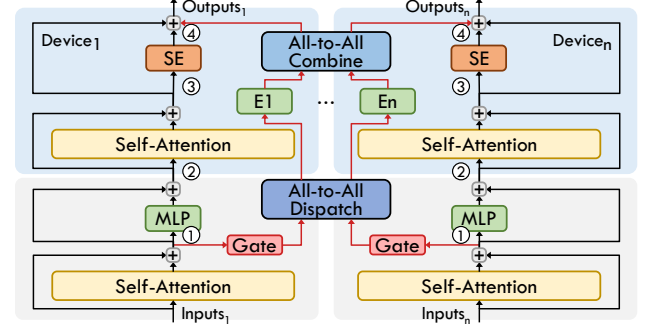


Figure 5. An overview of advanced expert parallelism using our ScMoE architecture and overlapping strategy. The red line represents the decoupled MoE stream and the numbers ① through ④ denote the potential locations for expert computation.

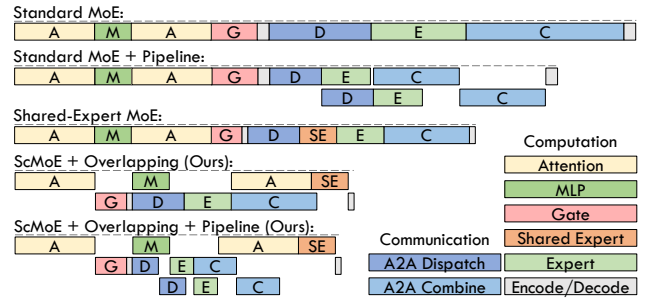


Figure 6. The timeline of different MoE architectures with corresponding parallel strategies, including pipeline and our proposed Overlapping. In each timeline, the length of each operator represents its time cost, while multiple rows indicate the utilization of parallel CUDA streams. The standard MoE utilizes top-2 gating, whereas the shared-expert MoE and ScMoE activate one shared expert alongside one gate-selected expert.

3.2 Overlapping Strategy for Expert Parallelism

As mentioned in the previous section, the MoE operations in ScMoE architecture are completely decoupled from the backbone network, enabling parallel execution across two independent streams: one for the shared expert process and another for the MoE process. To enhance the efficiency, we implement asynchronous All-to-All communication operators to enable the overlapping of communication and computation within these streams, while computation operators are unable to execute concurrently due to the constraints on computing resources.

Adaptive Operators Scheduling. We observe that operator execution times are influenced by the specific model and hardware configuration, necessitating the implementation of adaptive scheduling for operators.

Following the execution order in the MoE stream, we can directly schedule the gate routing and encode operators at the earliest viable position while deferring the decode operator to the latest position, thereby maximizing the potential

duration for overlapping. Then, this challenge is distilled into the selection of an optimal position for expert computation among four possible locations ①②③④ within the shared expert stream, as depicted in Figure 5.

Formally, we define the communication costs associated with ‘‘All-to-All Dispatch’’ and ‘‘All-to-All Combine’’ as \mathcal{T}_{disp} and \mathcal{T}_{comb} , respectively. The variable \mathcal{K} is designated to represent the specific location where expert computation is applied. Prior to the expert computation, the computational costs are denoted as $\mathcal{T}_{comp}^{pre} := \{COMP_1, \dots, COMP_{\mathcal{K}-1}\}$, while the costs following the expert computation are represented as $\mathcal{T}_{comp}^{post} := \{COMP_{\mathcal{K}+1}, \dots, COMP_4\}$. Consequently, the minimal aggregate time cost for each pair consisting of one Block-MLP and one Block-MoE is

$$\begin{aligned} \mathcal{T}_{overall}^{block} &= \min_{\mathcal{K}} (|\mathcal{T}_{comp}^{pre} - \mathcal{T}_{disp}| + |\mathcal{T}_{comp}^{post} - \mathcal{T}_{comb}|) \\ &= \min_{\mathcal{K}} (|\sum_{i=1}^{\mathcal{K}-1} COMP_i - \mathcal{T}_{disp}| + |\sum_{i=\mathcal{K}+1}^4 COMP_i - \mathcal{T}_{comb}|) \end{aligned} \quad (11)$$

$$\mathcal{T}_{overall}^{block} \geq |(\mathcal{T}_{comp}^{pre} + \mathcal{T}_{comp}^{post}) - (\mathcal{T}_{disp} + \mathcal{T}_{comb})| \quad (12)$$

$$\mathcal{T}_{overall}^{block} \leq (\mathcal{T}_{comp}^{pre} + \mathcal{T}_{comp}^{post}) + (\mathcal{T}_{disp} + \mathcal{T}_{comb}) \quad (13)$$

To demonstrate the efficiency, we have illustrated the operational timelines of various MoE architectures alongside their respective parallel strategies in Figure 6, exemplified by the selection of location ② for expert computation. Each timeline’s operator length corresponds to its execution time, and the presence of multiple rows signifies the utilization of parallel CUDA streams.

The widely-used pipeline parallel strategy equally segments input tokens into smaller fine-grained chunks, enabling concurrent computation and communication dispatched on distinct GPU streams (Hwang et al., 2022; Zhang et al., 2023). Contrary to standard MoE with pipelining (2nd timeline), our ScMoE with our proposed overlapping strategy (4th timeline) reduces the total communication time by half, leading to the same cost as the shared-expert MoE (3rd timeline). Our approach further optimizes performance by overlapping communication with the computation duration ($\mathcal{T}_{Atten} + \mathcal{T}_{SE} + \mathcal{T}_{MLP}$), which extends beyond the duration of expert computation achieved through pipelining.

Our strategy possesses the capability to fully overlap communication if the communication tasks can be accommodated within the overlapping window. This advantage is not shared by the pipeline strategy as it cannot overlap initial and terminal data transmissions (Huang et al., 2019; Narayanan et al., 2019). In cases where communication durations exceed the available overlap duration, our strategy can be augmented with pipelining (5th timeline), thereby utilizing the expert computation duration to further hide communication.

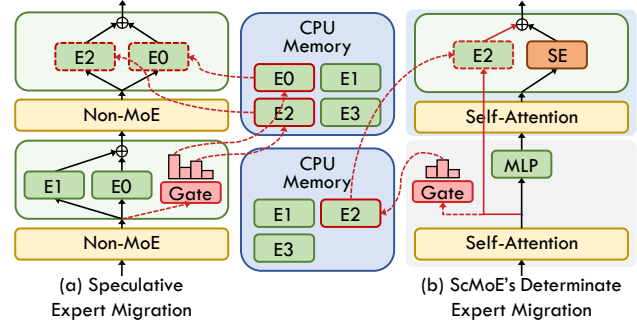


Figure 7. Illustrations of various expert migration methods to improve the efficiency of expert offloading: (a) speculative expert migration, exemplified by Pre-gated MoE (Hwang et al., 2023a), and (b) our ScMoE’s determinate expert migration. The red dashed line indicates expert selection and the transfer of expert parameters from CPU memory to GPU memory, while the black or red solid lines represent the data flow of representations processed by the Attention, MLP, and expert modules.

3.3 Expert Offloading Strategy for Memory-Limited Inference

As discussed in Section 2.3, MoE models encounter significant deployment challenges during on-device inference due to their model size exceeding GPU memory capacity, necessitating the offloading of expert parameters to CPU memory. Moreover, decoder-only models use an autoregressive process for natural language generation (NLG) inference tasks, allowing for per-token processing of MoE. Specifically, only the two activated experts (top-2 gating) for each token need to be transferred from CPU to GPU memory for computation, thereby reducing peak GPU memory usage.

To minimize the overhead caused by migrating activated expert parameters from CPU to GPU, speculative expert migration methods, represented by Pre-gated MoE (Hwang et al., 2023a), use preceding-layer representations to predict expert selection, as illustrated in Figure 7 (a). This approach allows the overlap of expert migration duration with the computation of preceding modules. Moreover, speculative expert migration methods adjust only the expert selection process, while expert computation continues along the same data flow of representations as in standard MoE.

In contrast, our proposed ScMoE architecture utilizes the gate-selected expert to compute the preceding-layer representations, inherently facilitating early expert migration well before the expert computation in the current layer. Based on this, we implement an expert offloading strategy that keeps non-expert and shared expert modules in GPU memory while offloading other gate-selected experts to CPU memory. After the Attention module in the preceding layer generates intermediate representations, the gate determines expert selection and issues asynchronous migration of the activated expert, as illustrated in Figure 7 (b). This approach

allows expert migration to overlap with the computation duration ($\mathcal{T}_{Atten} + \mathcal{T}_{SE} + \mathcal{T}_{MLP}$). Importantly, expert selection in our method adheres to the logic of the pre-trained ScMoE model, without any speculation.

Additionally, existing expert migration methods cannot be adapted to overlap communication in expert parallelism. This is because they do not decouple dependencies in the data flow of expert processing representations, and therefore cannot adjust the All-to-All communication of these representations.

4 EXPERIMENTS

4.1 Experimental Setup

Hardware Configurations. To assess the effectiveness of our proposed overlapping strategy for enhancing expert parallelism, we conduct experiments on three hardware configurations: $8 \times A30$ -PCIe, $8 \times A800$ -NVLink and $16 \times A800$ -NVLink (across 2 nodes). These configurations cover scenarios with both high and low communication-to-computation ratios. Additionally, we evaluate our proposed expert offloading strategy on a configuration with a single A30-PCIe GPU.

Experiments on Vision Model. To evaluate the efficacy of our MoE architectures on vision tasks, we conduct experiments on SwinV2-MoE model, which is a state-of-the-art vision transformer model built upon the Tutel MoE framework (Hwang et al., 2022; Liu et al., 2021). Specifically, we pre-train the SwinV2-MoE models with various MoE architectures on ImageNet-1K image classification dataset, and subsequently evaluate their accuracy on the corresponding test set. It is noteworthy that the integration of the MoE module within SwinV2 is confined to stages 3 and 4, with our architectural enhancements being selectively applied to the MoE modules in stage 3—the deepest submodel. Given our hardware constraints, we configure each MoE module with 8 experts, assigning one expert per GPU device.

Experiments on Language Model. For natural language generation (NLG) tasks, we utilize the standard implementations of GPT-2 (Radford et al., 2019) and GPT-3 (Brown et al., 2020) from Fairseq (Ott et al., 2019), augmented with Tutel MoE to construct GPT2-MoE and GPT3-MoE models featuring an 8-expert MoE module. Specifically, we implement it by substituting the MLP with MoE in the second transformer block of every consecutive pair. Then, we pre-train the models with different architectures on the OpenWebtext dataset (Gokaslan & Cohen, 2019). In addition to assessing the pre-training validation perplexity, we also conduct a zero-shot evaluation of the pre-trained model on the WikiText-103 (Merity et al., 2016) dataset.

More setup details are illustrated in Appendix A.6

Table 2. Test top-1 accuracy and end-to-end speedup of train and inference (one iteration) for SwinV2-MoE-S (Hwang et al., 2022) models with various architectures pre-trained on ImageNet-1K for 90 epochs in $8 \times A30$ -PCIe scenario, using standard MoE with top-2 gating as the baseline.

Model	ImageNet-1K (Acc@1↑)	Train (Speedup↑)	Inference (Speedup↑)
Standard top-2 MoE	79.33%	1	1
Standard top-1 MoE	78.95%	1.27×	1.39×
Shared-Expert MoE	79.53%	1.24×	1.35×
Our ScMoE	79.38%	1.43×	1.66×

Table 3. Comparison of zero-shot perplexity on WikiText-103 and end-to-end speedup analysis of train and inference (one iteration) for our pre-trained GPT2-MoE-Medium (Radford et al., 2019) models with various architectures in $8 \times A800$ -NVLink scenario, using standard top-2 MoE as the baseline.

Model	WikiText-103 (Perplexity↓)	Train (Speedup↑)	Inference (Speedup↑)
Standard top-2 MoE	19.18	1	1
Shared-Expert MoE	17.94	1.04×	1.06×
Our ScMoE	17.62	1.12×	1.17×

4.2 Analysis of Model Quality and Efficiency in Distributed Scenarios

In this section, we assess the model quality of our proposed ScMoE, which is a novel architectural design distinct from existing MoE models. Furthermore, we evaluate the efficiency of our ScMoE models in distributed scenarios, which are accelerated through our proposed overlapping strategy for enhancing expert parallelism. To maintain the same computational volume as the standard top-2 MoE, both the experimental Shared-Expert MoE and our ScMoE utilize one shared expert and one gate-selected expert.

4.2.1 Vision Model

Table 2 shows that our ScMoE and the standard top-2 MoE attain a comparable accuracy of 79.3%, while the shared-expert MoE delivers the highest accuracy, with a marginal increase of 0.2%. These methods, which utilize two activated experts, consistently outperform the standard top-1 MoE in terms of model quality, as the top-1 approach involves fewer parameters for computation.

Notably, in the $8 \times A30$ -PCIe scenario where communication overhead accounts for 60% of the total MoE time, our ScMoE model exhibits 30% speed improvement in training and 40% in inference compared to the standard top-2 MoE. Furthermore, it even surpasses the top-1 MoE by 13% in training speed and 20% in inference speed.

Consequently, our proposed ScMoE architecture improves the MoE models’ operational efficiency without compromising on model quality. Additional experiments with the

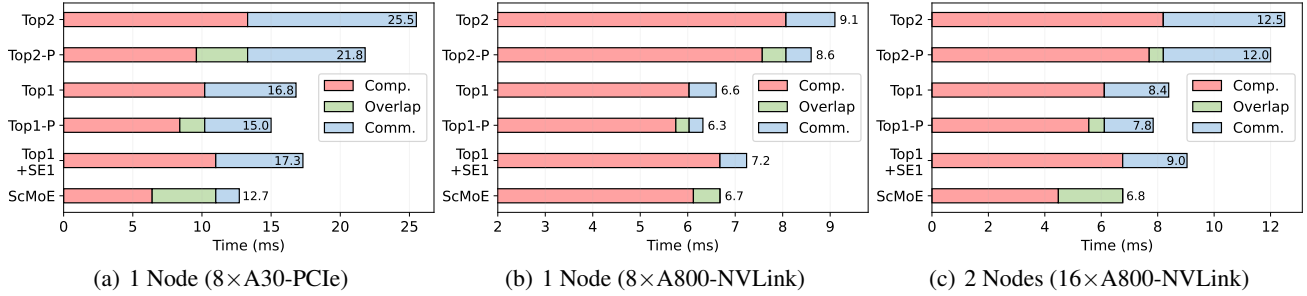


Figure 8. Overhead analysis for each pair of Block-MLP and Block-MoE within SwinV2-MoE-S model, deployed across three different distributed scenarios. “Topk” denotes the standard top-k MoE, while the one followed by the suffix “P” indicates using pipeline optimization as implemented by Tutel (Hwang et al., 2022). “Top1+SE1” refers to the shared-expert MoE.

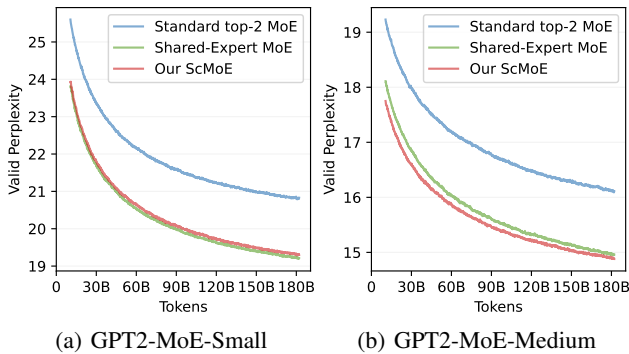


Figure 9. Token-wise validation perplexity curves for training MoE models with different MoE architectures.

SwinV2-MoE-B model demonstrate similar results, as detailed in Appendix A.4.

4.2.2 Language Model

As illustrated in Figure 9, both our ScMoE and the shared-expert MoE, which utilize one shared expert, demonstrate lower validation perplexity curves compared to the standard top-2 MoE during training on both the GPT2-MoE-Small and GPT2-MoE-Medium models. Consistently, in zero-shot evaluations on the WikiText-103 dataset (see Table 3), these two methods yield lower perplexity scores, with our ScMoE achieving 17.62 and the shared-expert MoE reaching 17.94, in contrast to the standard top-2 MoE, which results in a perplexity of 19.18.

As exemplified by the performance of GPT2-MoE-Small and GPT2-MoE-Medium models, our ScMoE performs high model quality across a range of network depths. Notably, our ScMoE demonstrates a superior training curve and zero-shot perplexity compared to the shared-expert MoE in the GPT2-MoE-Medium model, while the shared-expert MoE exhibits a slightly better training curve in the GPT2-MoE-Small model. This suggests that our ScMoE may offer greater benefits in deeper networks, aligning with our theoretical analysis of the shortcut connections, as detailed in

Appendix A.1. Additional zero-shot results of GPT2-MoE-Small are presented in Appendix A.4.

In addition, our ScMoE achieves 11% speed improvement in training and 15% in inference compared to standard top-2 MoE in the 8x A800-NVLink scenario, where communication constitutes 15% of the total MoE time.

4.2.3 Analysis of Overhead and Acceleration

In addition to exhibiting the significant end-to-end speedup of our ScMoE in Tables 2 and 3, we delve into a detailed analysis of the overhead and the acceleration effect with our overlapping strategy, which can be generalized to other Transformer-based MoE models.

In the communication-intensive 8x A30-PCIe scenario (Figure 8a), our ScMoE overlaps 70% communication time, resulting in a 27% speed improvement over shared-expert MoE, a 42% improvement over the pipelined standard top-2 MoE, and a 15% improvement over the pipelined standard top-1 MoE. In the 8x A800-NVLink scenario (Figure 8b), which features almost minimal communication overhead, our approach maintains its acceleration by completely overlapping communication.

In the multi-node distributed scenario (Figure 8c), with 16x A800-NVLink across two nodes, communication incurs more significant overhead than in the single-node 8x A800-NVLink scenario due to the lower-bandwidth inter-node Ethernet (Li et al., 2020). Here, our ScMoE achieves complete overlap, resulting in a 24% speed improvement over the shared-expert MoE, a 43% improvement over the pipelined standard top-2 MoE, and a 13% improvement over the pipelined standard top-1 MoE.

In general, our ScMoE delivers a significant acceleration over the standard top-2 MoE, and even outperforms the top-1 MoE when communication exceeds approximately 20% of the total MoE time. Additionally, our ScMoE can fully overlap communication in scenarios where communication does not exceed an estimated 50% of the total MoE time.

Table 4. Comparison of validation perplexity and end-to-end speedup analysis of train and inference (one iteration) for our pre-trained GPT3-MoE-XL (Brown et al., 2020) models with various architectures in $8\times$ A800-NVLink scenario, using standard MoE with top-2 gating as the baseline. “ScMoE-2” refers to the activation of one shared expert and two gate-selected experts.

Model	Validation (Perplexity↓)	Train (Speedup↑)	Inference (Speedup↑)
Standard top-2	17.52	1	1
Our ScMoE	16.46	1.12 \times	1.18 \times
Standard top-3	17.26	0.94 \times	0.92 \times
Our ScMoE-2	16.27	1.05 \times	1.08 \times

4.2.4 Analysis of More Activated Experts

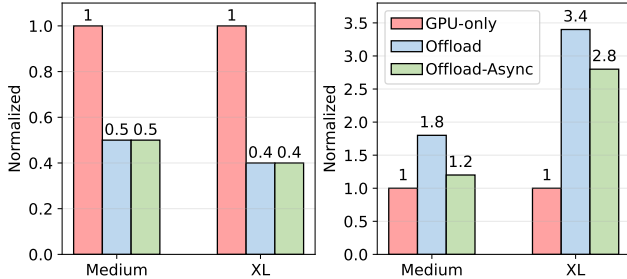
As increasing the number of activated experts within standard MoE is correlated with enhancements in model quality, we implement this augmentation in our ScMoE by increasing the count of gate-selected experts that process the preceding-layer representations, while maintaining the process of current-layer representations. To investigate the benefits of more activated experts, we implement the ScMoE-2, which employs top-2 experts for the preceding layer and one shared expert for the current layer.

Comparative analyses with the standard top-3 MoE, which has the same computational volumes as our ScMoE-2, reveal that our ScMoE architectures maintain superiority in both model quality and efficiency, as evidenced in Table 4. Furthermore, akin to the standard MoE, our ScMoE consistently improves with additional expert activation, shown by a decrease in validation perplexity from 16.46 with ScMoE to 16.27 with ScMoE-2.

Although activating more experts incurs higher time costs, the efficiency improvements of our overlapping strategy remain significant. For instance, our ScMoE-2 requires merely 95% and 93% of the time cost necessary for the standard top-2 MoE respectively in training and inference, despite processing increased computational loads.

4.3 Analysis of Memory-Limited Inference

To tackle the challenges of on-device inference, where it is not feasible to store the entire MoE model parameters in GPU memory, our strategy involves offloading gate-selected experts to CPU memory while retaining non-expert and shared expert modules in GPU memory. As demonstrated in Table 10 (a), our expert offloading strategy reduces peak GPU memory usage by 50% for the GPT2-MoE-Medium model and by 60% for the GPT3-MoE-XL model when deployed in the inference scenario using a single A30-PCIe GPU. Furthermore, it is anticipated that models with more gate-selected experts in each MoE module will experience a larger percentage reduction in GPU memory usage.



(a) Peak GPU Memory Usage (b) MoE Block Latency

Figure 10. Peak GPU memory usage (a) and MoE block latency (b) for various memory-limited inference methods applied to the GPT2-MoE-Medium and GPT3-MoE-XL models using ScMoE. “GPU-only” indicates that the entire model is stored in GPU memory. “Offload” refers to our strategy of offloading expert parameters to CPU with blocking expert migration. “Offload-Async” denotes the use of asynchronous expert migration to overlap its duration.

Since the offloaded expert parameters must be loaded into the GPU memory for expert computation, the blocking execution of this expert migration results in significant overhead. As shown in Table 10 (b), the blocking expert migration introduces an additional overhead of 80% in GPT2-MoE-Medium and 240% in GPT3-MoE-XL, substantially increasing the MoE block latency. To mitigate this issue, our strategy of asynchronously executing the determinate expert migration effectively reduces the additional costs by 75% in GPT2-MoE-Medium and 25% in GPT3-MoE-XL.

Furthermore, it is evident that expanding the model size from Medium to XL significantly raises the cost proportion related to expert migration. This is because the per-token decoding process during inference is memory-bound (Patel et al., 2024; Wu et al., 2024). The larger model size leads to a proportional increase in the duration of memory transfer, without a corresponding increase in computation time.

4.4 Analysis of the Proposed Shortcut Connection

Our comprehensive empirical results have demonstrated that our ScMoE architecture facilitates efficiency optimizations without compromising model quality. We further explore the proposed shortcut connection in greater depth, uncovering the reasons behind its algorithmic effectiveness.

Firstly, we investigate the use of the same MoE module to select the top-1 expert twice for processing each input token’s current-layer and preceding-layer representations, respectively. As illustrated in Figure 11 (a), we observe that the same gating network typically selects the same expert for the two representations of most tokens. As the training progresses, the token percentage of repeating selection initially escalates, peaking at 98%, and then diminishes, with a significant drop manifested in the last MoE sub-layer.

Next, we measure the L2 distance (similarity) between each

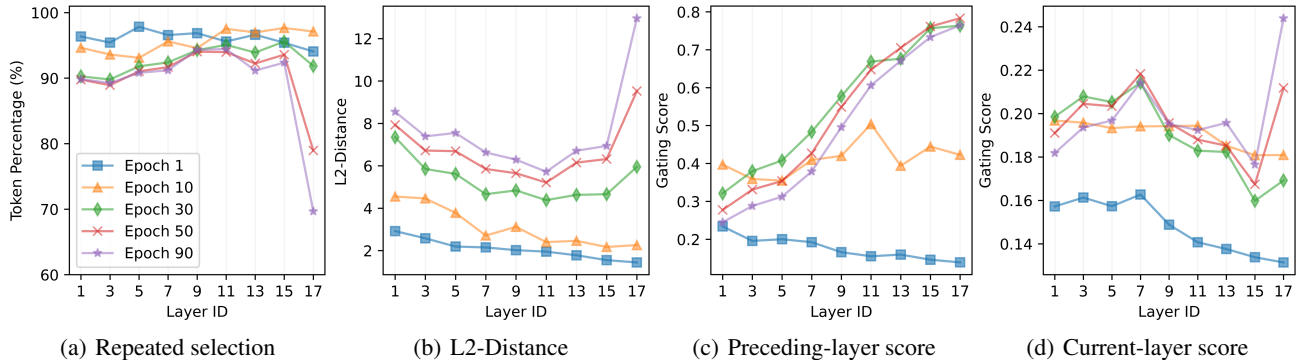


Figure 11. Results from the analysis of the proposed shortcut connection, during the 90-epoch training (including a 10-epoch warm-up) of the SwinV2-MoE-S model (Hwang et al., 2022). Employing the same MoE module to select the top-1 expert twice for processing each input token’s two representations from the current and preceding layers, respectively, (a) illustrates the percentage of tokens that retain the same expert selection across the current layer and preceding layer, (b) shows the L2 distance between these two representations. Using the DGMoE, which imposes a constraint against repeatedly selecting the same expert, (c) presents the average gating score for the preceding-layer representations, (d) displays the average gating score for the current-layer representations.

token’s preceding-layer and current-layer representations. Figure 11 (b) illustrates that, as training advances, the L2 similarity initially decreases with network depth, then increases, and ultimately reaches its maximum value in the final layer. Since the gating network is used to classify the representations, this similarity may lead to the repeated selection of the same experts, as evidenced by the correlation between the results in Figure 11 (a) and (b).

Notably, we observe this experimental architecture only achieves model quality on par with the standard top-1 MoE, despite incurring the same computational cost as the top-2 MoE. To address this, we impose a constraint on the MoE module to ensure that it selects a different expert for the current layer than the one chosen for the preceding layer. We refer to this enhanced experimental architecture as DoubleGating MoE (DGMoE), which achieves model quality comparable to standard top-2 MoE by imposing the constraint against selecting the same expert repeatedly.

With this constraint, we observe gating score behaviors are similar to those of the standard top-2 MoE (Riquelme et al., 2021), as illustrated in Figure 11 (c) and (d). Specifically, in (c), the gating scores associated with representations from preceding layers grow quickly initially, converging thereafter, and achieving their maximum in the final MoE sub-layer. By comparison, in (d), the gating scores of current layer across all MoE sub-layers are around 0.2 (± 0.04), lower than the 0.2 to 0.8 range for that of preceding layer.

In summary, the experiments indicate that the combined results of two representations, produced by the same expert, are approximately equivalent to those obtained by using a single expert to process only the current-layer representations. This equivalence may arise from the similarity between the preceding-layer and current-layer representations of each token. Furthermore, enforcing two distinct experts

can enable the DGMoE architecture to achieve behaviors and model quality similar to those of a standard top-2 MoE.

Analogously, our ScMoE architecture has already allocated distinct experts for the two representations of each token, thereby maintaining a similar behavior to the shared-expert MoE architecture and ensuring comparable model quality. Given the differences between standard MoE and shared-expert MoE, we have observed that DGMoE achieves accuracy levels closer to those of the standard top-2 MoE, while ScMoE aligns more closely with shared-expert MoE, as demonstrated in the results presented in Appendix A.2.

Additionally, our ScMoE model may leverage the differences between the representations of preceding layers and those of the current layer, while still preserving significant similarities. This distinction potentially provides additional information that enhances the training of MoE models, especially considering that MoE models typically require larger training datasets compared to dense MLP models (Artetxe et al., 2022; Fedus et al., 2022; Xue et al., 2022).

5 CONCLUSION

The inherent dependencies of communication in distributed MoE models hinder parallel optimization techniques to improve execution efficiency. To overcome this, we propose a novel shortcut-connected MoE (ScMoE) architecture, and develop a communication overlapping parallel strategy. Through comprehensive empirical evaluation and theoretical analysis, our approaches demonstrate better execution efficiency while maintaining, or exceeding, the model quality of existing methods. Moreover, we further implement an expert offloading strategy upon our ScMoE to enable memory-limited inference and optimize latency by overlapping expert migration. Additionally, we provide insightful analysis and discussion on our proposed MoE architecture.

REFERENCES

- Achiam, J., Adler, S., Agarwal, S., Ahmad, L., Akkaya, I., Aleman, F. L., Almeida, D., Altenschmidt, J., Altman, S., Anadkat, S., et al. Gpt-4 technical report. *arXiv preprint arXiv:2303.08774*, 2023.
- Artetxe, M., Bhosale, S., Goyal, N., Mihaylov, T., Ott, M., Shleifer, S., Lin, X. V., Du, J., Iyer, S., Pasunuru, R., Anantharaman, G., Li, X., Chen, S., Akin, H., Baines, M., Martin, L., Zhou, X., Koura, P. S., O’Horo, B., Wang, J., Zettlemoyer, L., Diab, M. T., Kozareva, Z., and Stoyanov, V. Efficient large scale language modeling with mixtures of experts. In Goldberg, Y., Kozareva, Z., and Zhang, Y. (eds.), *Proceedings of the 2022 Conference on Empirical Methods in Natural Language Processing, EMNLP 2022, Abu Dhabi, United Arab Emirates, December 7-11, 2022*, pp. 11699–11732. Association for Computational Linguistics, 2022. doi: 10.18653/V1/2022.EMNLP-MAIN.804. URL <https://doi.org/10.18653/v1/2022.emnlp-main.804>.
- Brown, T., Mann, B., Ryder, N., Subbiah, M., Kaplan, J. D., Dhariwal, P., Neelakantan, A., Shyam, P., Sastry, G., Askell, A., et al. Language models are few-shot learners. *Advances in neural information processing systems*, 33: 1877–1901, 2020.
- Chen, S., Jie, Z., and Ma, L. Llava-mole: Sparse mixture of lora experts for mitigating data conflicts in instruction finetuning mllms. *arXiv preprint arXiv:2401.16160*, 2024.
- Chowdhery, A., Narang, S., Devlin, J., Bosma, M., Mishra, G., Roberts, A., Barham, P., Chung, H. W., Sutton, C., Gehrmann, S., et al. Palm: Scaling language modeling with pathways. *Journal of Machine Learning Research*, 24(240):1–113, 2023.
- Dai, D., Deng, C., Zhao, C., Xu, R., Gao, H., Chen, D., Li, J., Zeng, W., Yu, X., Wu, Y., et al. Deepseekmoe: Towards ultimate expert specialization in mixture-of-experts language models. *arXiv preprint arXiv:2401.06066*, 2024.
- Dehghani, M., Gouws, S., Vinyals, O., Uszkoreit, J., and Kaiser, L. Universal transformers. In *International Conference on Learning Representations*, 2018.
- Dosovitskiy, A., Beyer, L., Kolesnikov, A., Weissenborn, D., Zhai, X., Unterthiner, T., Dehghani, M., Minderer, M., Heigold, G., Gelly, S., Uszkoreit, J., and Houlsby, N. An image is worth 16x16 words: Transformers for image recognition at scale. In *9th International Conference on Learning Representations, ICLR 2021, Virtual Event, Austria, May 3-7, 2021*. OpenReview.net, 2021. URL <https://openreview.net/forum?id=YicbFdNTTy>.
- Du, N., Huang, Y., Dai, A. M., Tong, S., Lepikhin, D., Xu, Y., Krikun, M., Zhou, Y., Yu, A. W., Firat, O., Zoph, B., Fedus, L., Bosma, M. P., Zhou, Z., Wang, T., Wang, Y. E., Webster, K., Pellat, M., Robinson, K., Meier-Hellstern, K. S., Duke, T., Dixon, L., Zhang, K., Le, Q. V., Wu, Y., Chen, Z., and Cui, C. Glam: Efficient scaling of language models with mixture-of-experts. In Chaudhuri, K., Jegelka, S., Song, L., Szepesvári, C., Niu, G., and Sabato, S. (eds.), *International Conference on Machine Learning, ICML 2022, 17-23 July 2022, Baltimore, Maryland, USA*, volume 162 of *Proceedings of Machine Learning Research*, pp. 5547–5569. PMLR, 2022. URL <https://proceedings.mlr.press/v162/du22c.html>.
- Du, Z., Li, S., Wu, Y., Jiang, X., Sun, J., Zheng, Q., Wu, Y., Li, A., Li, H., and Chen, Y. Sida: Sparsity-inspired data-aware serving for efficient and scalable large mixture-of-experts models. *Proceedings of Machine Learning and Systems*, 6:224–238, 2024.
- Fedus, W., Zoph, B., and Shazeer, N. Switch transformers: Scaling to trillion parameter models with simple and efficient sparsity. *The Journal of Machine Learning Research*, 23(1):5232–5270, 2022.
- Foley, D. and Danskin, J. Ultra-performance pascal GPU and nvlinc interconnect. *IEEE Micro*, 37(2):7–17, 2017. doi: 10.1109/MM.2017.37. URL <https://doi.org/10.1109/MM.2017.37>.
- Gao, C., Chen, K., Rao, J., Sun, B., Liu, R., Peng, D., Zhang, Y., Guo, X., Yang, J., and Subrahmanian, V. Higher layers need more lora experts. *arXiv preprint arXiv:2402.08562*, 2024.
- Gokaslan, A. and Cohen, V. Openwebtext corpus. <http://Skylion007.github.io/OpenWebTextCorpus>, 2019.
- Gou, Y., Liu, Z., Chen, K., Hong, L., Xu, H., Li, A., Yeung, D., Kwok, J. T., and Zhang, Y. Mixture of cluster-conditional lora experts for vision-language instruction tuning. *CoRR*, abs/2312.12379, 2023. doi: 10.48550/ARXIV.2312.12379. URL <https://doi.org/10.48550/arXiv.2312.12379>.
- He, J., Qiu, J., Zeng, A., Yang, Z., Zhai, J., and Tang, J. Fastmoe: A fast mixture-of-expert training system. *arXiv preprint arXiv:2103.13262*, 2021.
- He, J., Zhai, J., Antunes, T., Wang, H., Luo, F., Shi, S., and Li, Q. Fastermoe: modeling and optimizing training of large-scale dynamic pre-trained models. In Lee, J., Agrawal, K., and Spear, M. F. (eds.), *PPoPP ’22: 27th ACM SIGPLAN Symposium on Principles and Practice of Parallel Programming, Seoul, Republic of Korea, April 2 - 6, 2022*, pp. 120–134. ACM,

2022. doi: 10.1145/3503221.3508418. URL <https://doi.org/10.1145/3503221.3508418>.
- Huang, G., Liu, Z., van der Maaten, L., and Weinberger, K. Q. Densely connected convolutional networks. In *2017 IEEE Conference on Computer Vision and Pattern Recognition, CVPR 2017, Honolulu, HI, USA, July 21-26, 2017*, pp. 2261–2269. IEEE Computer Society, 2017. doi: 10.1109/CVPR.2017.243. URL <https://doi.org/10.1109/CVPR.2017.243>.
- Huang, Y., Cheng, Y., Bapna, A., Firat, O., Chen, D., Chen, M. X., Lee, H., Ngiam, J., Le, Q. V., Wu, Y., and Chen, Z. Gpipe: Efficient training of giant neural networks using pipeline parallelism. In Wallach, H. M., Larochelle, H., Beygelzimer, A., d’Alché-Buc, F., Fox, E. B., and Garnett, R. (eds.), *Advances in Neural Information Processing Systems 32: Annual Conference on Neural Information Processing Systems 2019, NeurIPS 2019, December 8-14, 2019, Vancouver, BC, Canada*, pp. 103–112, 2019.
- Hwang, C., Cui, W., Xiong, Y., Yang, Z., Liu, Z., Hu, H., Wang, Z., Salas, R., Jose, J., Ram, P., Chau, J., Cheng, P., Yang, F., Yang, M., and Xiong, Y. Tutel: Adaptive mixture-of-experts at scale. *CoRR*, abs/2206.03382, 2022. doi: 10.48550/ARXIV.2206.03382. URL <https://doi.org/10.48550/arXiv.2206.03382>.
- Hwang, R., Wei, J., Cao, S., Hwang, C., Tang, X., Cao, T., Yang, M., and Rhu, M. Pre-gated moe: An algorithm-system co-design for fast and scalable mixture-of-expert inference. *CoRR*, abs/2308.12066, 2023a. doi: 10.48550/ARXIV.2308.12066. URL <https://doi.org/10.48550/arXiv.2308.12066>.
- Hwang, R., Wei, J., Cao, S., Hwang, C., Tang, X., Cao, T., Yang, M., and Rhu, M. Pre-gated moe: An algorithm-system co-design for fast and scalable mixture-of-expert inference. *arXiv preprint arXiv:2308.12066*, 2023b.
- Jiang, A. Q., Sablayrolles, A., Roux, A., Mensch, A., Savary, B., Bamford, C., Chaplot, D. S., Casas, D. d. I., Hanna, E. B., Bressand, F., et al. Mixtral of experts. *arXiv preprint arXiv:2401.04088*, 2024.
- Lan, Z., Chen, M., Goodman, S., Gimpel, K., Sharma, P., and Soricut, R. Albert: A lite bert for self-supervised learning of language representations. In *International Conference on Learning Representations*, 2019.
- Lepikhin, D., Lee, H., Xu, Y., Chen, D., Firat, O., Huang, Y., Krikun, M., Shazeer, N., and Chen, Z. Gshard: Scaling giant models with conditional computation and automatic sharding. In *9th International Conference on Learning Representations, ICLR 2021, Virtual Event, Austria, May 3-7, 2021*. OpenReview.net, 2021. URL <https://openreview.net/forum?id=qrwe7XHTmYb>.
- Li, A., Song, S. L., Chen, J., Li, J., Liu, X., Tallent, N. R., and Barker, K. J. Evaluating modern GPU interconnect: Pcie, nvlLink, nv-sli, nvswitch and gpudirect. *IEEE Trans. Parallel Distributed Syst.*, 31(1):94–110, 2020. doi: 10.1109/TPDS.2019.2928289. URL <https://doi.org/10.1109/TPDS.2019.2928289>.
- Liu, Z., Lin, Y., Cao, Y., Hu, H., Wei, Y., Zhang, Z., Lin, S., and Guo, B. Swin transformer: Hierarchical vision transformer using shifted windows. In *2021 IEEE/CVF International Conference on Computer Vision, ICCV 2021, Montreal, QC, Canada, October 10-17, 2021*, pp. 9992–10002. IEEE, 2021. doi: 10.1109/ICCV48922.2021.00986. URL <https://doi.org/10.1109/ICCV48922.2021.00986>.
- Lu, J., Batra, D., Parikh, D., and Lee, S. Vilbert: Pretraining task-agnostic visiolinguistic representations for vision-and-language tasks. In Wallach, H. M., Larochelle, H., Beygelzimer, A., d’Alché-Buc, F., Fox, E. B., and Garnett, R. (eds.), *Advances in Neural Information Processing Systems 32: Annual Conference on Neural Information Processing Systems 2019, NeurIPS 2019, December 8-14, 2019, Vancouver, BC, Canada*, pp. 13–23, 2019.
- Mayer, R. and Jacobsen, H.-A. Scalable deep learning on distributed infrastructures: Challenges, techniques, and tools. *ACM Computing Surveys (CSUR)*, 53(1):1–37, 2020.
- Merity, S., Xiong, C., Bradbury, J., and Socher, R. Pointer sentinel mixture models. *arXiv preprint arXiv:1609.07843*, 2016.
- Mustafa, B., Riquelme, C., Puigcerver, J., Jenatton, R., and Hounsby, N. Multimodal contrastive learning with limoe: the language-image mixture of experts. In Koyejo, S., Mohamed, S., Agarwal, A., Belgrave, D., Cho, K., and Oh, A. (eds.), *Advances in Neural Information Processing Systems 35: Annual Conference on Neural Information Processing Systems 2022, NeurIPS 2022, New Orleans, LA, USA, November 28 - December 9, 2022*, 2022.
- Narayanan, D., Harlap, A., Phanishayee, A., Seshadri, V., Devanur, N. R., Ganger, G. R., Gibbons, P. B., and Zaharia, M. Pipedream: generalized pipeline parallelism for DNN training. In Brecht, T. and Williamson, C. (eds.), *Proceedings of the 27th ACM Symposium on Operating Systems Principles, SOSP 2019, Huntsville, ON, Canada, October 27-30, 2019*, pp. 1–15. ACM, 2019. doi: 10.1145/3341301.3359646. URL <https://doi.org/10.1145/3341301.3359646>.
- Narayanan, D., Shoeybi, M., Casper, J., LeGresley, P., Patwary, M., Korthikanti, V., Vainbrand, D., Kashinkunti, P., Bernauer, J., Catanzaro, B., Phanishayee, A., and

- Zaharia, M. Efficient large-scale language model training on GPU clusters using megatron-lm. In de Supinski, B. R., Hall, M. W., and Gamblin, T. (eds.), *International Conference for High Performance Computing, Networking, Storage and Analysis, SC 2021, St. Louis, Missouri, USA, November 14-19, 2021*, pp. 58. ACM, 2021. doi: 10.1145/3458817.3476209. URL <https://doi.org/10.1145/3458817.3476209>.
- Nie, X., Zhao, P., Miao, X., Zhao, T., and Cui, B. Hetumoe: An efficient trillion-scale mixture-of-expert distributed training system. *CoRR*, abs/2203.14685, 2022. doi: 10.48550/ARXIV.2203.14685. URL <https://doi.org/10.48550/arXiv.2203.14685>.
- Ott, M., Edunov, S., Baevski, A., Fan, A., Gross, S., Ng, N., Grangier, D., and Auli, M. fairseq: A fast, extensible toolkit for sequence modeling. *arXiv preprint arXiv:1904.01038*, 2019.
- Ouyang, L., Wu, J., Jiang, X., Almeida, D., Wainwright, C., Mishkin, P., Zhang, C., Agarwal, S., Slama, K., Ray, A., et al. Training language models to follow instructions with human feedback. *Advances in Neural Information Processing Systems*, 35:27730–27744, 2022.
- Patel, P., Choukse, E., Zhang, C., Shah, A., Goiri, Í., Maleki, S., and Bianchini, R. Splitwise: Efficient generative llm inference using phase splitting. In *2024 ACM/IEEE 51st Annual International Symposium on Computer Architecture (ISCA)*, pp. 118–132. IEEE, 2024.
- Radford, A., Wu, J., Child, R., Luan, D., Amodei, D., Sutskever, I., et al. Language models are unsupervised multitask learners. *OpenAI blog*, 1(8):9, 2019.
- Rajbhandari, S., Rasley, J., Ruwase, O., and He, Y. Zero: Memory optimizations toward training trillion parameter models. In *SC20: International Conference for High Performance Computing, Networking, Storage and Analysis*, pp. 1–16. IEEE, 2020.
- Rajbhandari, S., Ruwase, O., Rasley, J., Smith, S., and He, Y. Zero-infinity: Breaking the gpu memory wall for extreme scale deep learning. In *Proceedings of the International Conference for High Performance Computing, Networking, Storage and Analysis*, pp. 1–14, 2021.
- Rajbhandari, S., Li, C., Yao, Z., Zhang, M., Aminabadi, R. Y., Awan, A. A., Rasley, J., and He, Y. DeepSpeed-moe: Advancing mixture-of-experts inference and training to power next-generation ai scale. In *International Conference on Machine Learning*, pp. 18332–18346. PMLR, 2022.
- Riquelme, C., Puigcerver, J., Mustafa, B., Neumann, M., Jenatton, R., Pinto, A. S., Keysers, D., and Houlsby, N. Scaling vision with sparse mixture of experts. In Ranzato, M., Beygelzimer, A., Dauphin, Y. N., Liang, P., and Vaughan, J. W. (eds.), *Advances in Neural Information Processing Systems 34: Annual Conference on Neural Information Processing Systems 2021, NeurIPS 2021, December 6-14, 2021, virtual*, pp. 8583–8595, 2021.
- Shazeer, N., Mirhoseini, A., Maziarz, K., Davis, A., Le, Q. V., Hinton, G. E., and Dean, J. Outrageously large neural networks: The sparsely-gated mixture-of-experts layer. In *5th International Conference on Learning Representations, ICLR 2017, Toulon, France, April 24-26, 2017, Conference Track Proceedings*. OpenReview.net, 2017. URL <https://openreview.net/forum?id=BlckMDqlg>.
- Shen, L., Wu, Z., Gong, W., Hao, H., Bai, Y., Wu, H., Wu, X., Bian, J., Xiong, H., Yu, D., et al. Se-moe: A scalable and efficient mixture-of-experts distributed training and inference system. *arXiv preprint arXiv:2205.10034*, 2022.
- Shen, S., Yao, Z., Li, C., Darrell, T., Keutzer, K., and He, Y. Scaling vision-language models with sparse mixture of experts. *arXiv preprint arXiv:2303.07226*, 2023.
- Singh, S., Ruwase, O., Awan, A. A., Rajbhandari, S., He, Y., and Bhatle, A. A hybrid tensor-expert-data parallelism approach to optimize mixture-of-experts training. In Gallivan, K. A., Gallopoulos, E., Nikolopoulos, D. S., and Bevide, R. (eds.), *Proceedings of the 37th International Conference on Supercomputing, ICS 2023, Orlando, FL, USA, June 21-23, 2023*, pp. 203–214. ACM, 2023. doi: 10.1145/3577193.3593704. URL <https://doi.org/10.1145/3577193.3593704>.
- Smith, S., Patwary, M., Norick, B., LeGresley, P., Rajbhandari, S., Casper, J., Liu, Z., Prabhume, S., Zerveas, G., Korthikanti, V., Zheng, E., Child, R., Aminabadi, R. Y., Bernauer, J., Song, X., Shoyebi, M., He, Y., Houston, M., Tiwary, S., and Catanzaro, B. Using deepspeed and megatron to train megatron-turing NLG 530b, A large-scale generative language model. *CoRR*, abs/2201.11990, 2022. URL <https://arxiv.org/abs/2201.11990>.
- Team, Q. “Qwen1.5-MoE: Matching 7B Model Performance with 1/3 Activated Parameters”, February 2024. URL <https://qwenlm.github.io/blog/qwen-moe/>.
- Vaswani, A., Shazeer, N., Parmar, N., Uszkoreit, J., Jones, L., Gomez, A. N., Kaiser, L., and Polosukhin, I. Attention is all you need. In Guyon, I., von Luxburg, U., Bengio, S., Wallach, H. M., Fergus, R., Vishwanathan, S. V. N., and Garnett, R. (eds.), *Advances in Neural Information Processing Systems 30: Annual Conference on Neural*

- Information Processing Systems 2017, December 4-9, 2017, Long Beach, CA, USA*, pp. 5998–6008, 2017.
- Wang, S., Wei, J., Sabne, A., Davis, A., Ilbeyi, B., Hechtman, B., Chen, D., Murthy, K. S., Maggioni, M., Zhang, Q., Kumar, S., Guo, T., Xu, Y., and Zhou, Z. Overlap communication with dependent computation via decomposition in large deep learning models. In Aamodt, T. M., Jerger, N. D. E., and Swift, M. M. (eds.), *Proceedings of the 28th ACM International Conference on Architectural Support for Programming Languages and Operating Systems, Volume 1, ASPLOS 2023, Vancouver, BC, Canada, March 25-29, 2023*, pp. 93–106. ACM, 2023. doi: 10.1145/3567955.3567959. URL <https://doi.org/10.1145/3567955.3567959>.
- Wei, J., Tay, Y., Bommasani, R., Raffel, C., Zoph, B., Borgeaud, S., Yogatama, D., Bosma, M., Zhou, D., Metzler, D., et al. Emergent abilities of large language models. *arXiv preprint arXiv:2206.07682*, 2022a.
- Wei, J., Wang, X., Schuurmans, D., Bosma, M., Xia, F., Chi, E., Le, Q. V., Zhou, D., et al. Chain-of-thought prompting elicits reasoning in large language models. *Advances in Neural Information Processing Systems*, 35: 24824–24837, 2022b.
- Wu, B., Liu, S., Zhong, Y., Sun, P., Liu, X., and Jin, X. Loongserve: Efficiently serving long-context large language models with elastic sequence parallelism. *arXiv preprint arXiv:2404.09526*, 2024.
- Wu, X., Huang, S., and Wei, F. Mole: Mixture of lora experts. In *The Twelfth International Conference on Learning Representations*, 2023.
- Xue, F., Shi, Z., Wei, F., Lou, Y., Liu, Y., and You, Y. Go wider instead of deeper. In *Proceedings of the AAAI Conference on Artificial Intelligence*, volume 36, pp. 8779–8787, 2022.
- Xue, F., Zheng, Z., Fu, Y., Ni, J., Zheng, Z., Zhou, W., and You, Y. Openmoe: An early effort on open mixture-of-experts language models. *arXiv preprint arXiv:2402.01739*, 2024.
- Yi, R., Guo, L., Wei, S., Zhou, A., Wang, S., and Xu, M. Edgemoe: Fast on-device inference of moe-based large language models. *arXiv preprint arXiv:2308.14352*, 2023.
- Zhang, P., Li, X., Hu, X., Yang, J., Zhang, L., Wang, L., Choi, Y., and Gao, J. Vinvl: Revisiting visual representations in vision-language models. In *Proceedings of the IEEE/CVF conference on computer vision and pattern recognition*, pp. 5579–5588, 2021.
- Zhang, Z., Yang, D., Xia, Y., Ding, L., Tao, D., Zhou, X., and Cheng, D. Mpipemoe: Memory efficient moe for pre-trained models with adaptive pipeline parallelism. In *IEEE International Parallel and Distributed Processing Symposium, IPDPS 2023, St. Petersburg, FL, USA, May 15-19, 2023*, pp. 167–177. IEEE, 2023. doi: 10.1109/IPDPS54959.2023.00026. URL <https://doi.org/10.1109/IPDPS54959.2023.00026>.
- Zheng, L., Li, Z., Zhang, H., Zhuang, Y., Chen, Z., Huang, Y., Wang, Y., Xu, Y., Zhuo, D., Xing, E. P., Gonzalez, J. E., and Stoica, I. Alpa: Automating inter- and intra-operator parallelism for distributed deep learning. In Aguilera, M. K. and Weatherspoon, H. (eds.), *16th USENIX Symposium on Operating Systems Design and Implementation, OSDI 2022, Carlsbad, CA, USA, July 11-13, 2022*, pp. 559–578. USENIX Association, 2022. URL <https://www.usenix.org/conference/osdi22/presentation/zheng-lianmin>.
- Zhou, K., Yang, J., Loy, C. C., and Liu, Z. Learning to prompt for vision-language models. *International Journal of Computer Vision*, 130(9):2337–2348, 2022.
- Zhu, D., Chen, J., Shen, X., Li, X., and Elhoseiny, M. Minigpt-4: Enhancing vision-language understanding with advanced large language models. *arXiv preprint arXiv:2304.10592*, 2023.

A APPENDIX

A.1 Theoretical Analysis

In this section, we delve deeper into the understanding of our proposed shortcut-connected MoE (ScMoE) architecture, presenting a theoretical foundation focused on the propagation of gradients to guarantee consistent training and preserve model quality. Our analysis is confined to our ScMoE architecture as depicted in Figure 4(b); however, the same principles and derivations can be easily extended to other shortcut-connected MoE architectures. Building upon Equations 7 to 10, we can derive

$$\begin{aligned} \mathcal{H}_{l+1} &= \mathcal{H}_l^{MH} + \left(\text{MLP}^{(l)}(\mathcal{H}_l^{MH}) \right. \\ &\quad + \text{MultiHead}^{(l+1)}(\mathcal{H}_l^{MH} + \text{MLP}^{(l)}(\mathcal{H}_l^{MH})) \\ &\quad + \text{SE}^{(l+1)}(\mathcal{H}_l^{MH} + \text{MLP}^{(l)}(\mathcal{H}_l^{MH})) \\ &\quad \left. + \text{MultiHead}^{(l+1)}(\mathcal{H}_l^{MH} + \text{MLP}^{(l)}(\mathcal{H}_l^{MH})) \right) \\ &\quad + \sum_{i=1}^N G(\mathcal{H}_l^{MH})_i E_i(\mathcal{H}_l^{MH}) \end{aligned} \quad (14)$$

$$\mathcal{H}_i^{MH} = \mathcal{H}_{i-1} + \text{MultiHead}^{(i)}(\mathcal{H}_{i-1}) \quad (15)$$

It is observable that Equations 14 and 15 share an identical structural expression. Consequently, we consider each pair of Block-MoE and Block-MLP layers as a single entity, and every sub-layer, denoted as \mathcal{F} , with its corresponding parameters \mathcal{W}_l , conforms to the equation

$$x_{l+1} = x_l + \mathcal{F}_{\mathcal{W}_l}(x_l) \quad (16)$$

Here, x_l represents the input, and x_{l+1} represents the output of the l -th sub-layer. By applying this relationship recursively, the output of the uppermost L -th sub-layer, x_L , can be deduced as follows

$$x_L = x_l + \sum_{i=l}^{L-1} \mathcal{F}_{\mathcal{W}_i}(x_i) \quad (17)$$

Let's consider the loss function as \mathcal{E} . Using the chain rule, we can calculate the derivative of the loss with respect to x_l , and we have

$$\frac{\partial \mathcal{E}}{\partial x_l} = \frac{\partial \mathcal{E}}{\partial x_L} \frac{\partial x_L}{\partial x_l} = \frac{\partial \mathcal{E}}{\partial x_L} \left(1 + \frac{\partial}{\partial x_l} \sum_{i=1}^{L-1} \mathcal{F}_{\mathcal{W}_i}(x_i) \right) \quad (18)$$

It's clear that the additive component of the error gradient $\frac{\partial \mathcal{E}}{\partial x_L}$ ensures direct information propagation back to any sub-layer x_l . Additionally, its advantage is that the number of product elements on the right side is independent of the network's depth. Therefore, as L increases, it is less likely to encounter the gradient vanishing or exploding problem, ensuring stable training and sustained performance levels in our proposed MoE architectures.

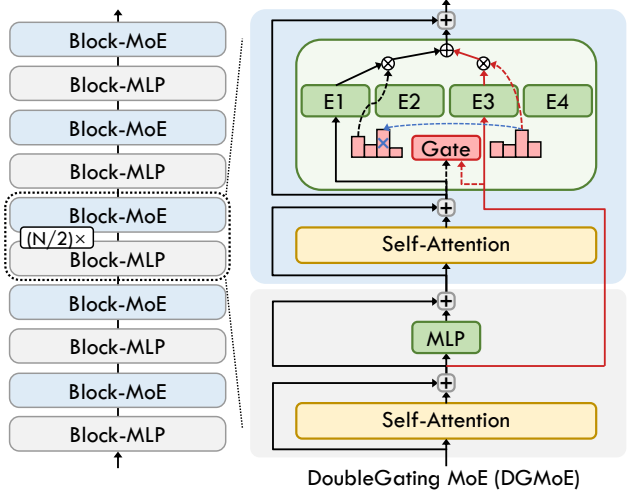


Figure 12. Illustration of the experimental DoubleGating MoE (DGMoE) architecture.

A.2 Analysis of the DoubleGating MoE (DGMoE)

To delve deeper into our architecture with shortcut connection, we introduce the DoubleGating MoE (DGMoE) architecture, which employs dual top-1 gating mechanisms to independently process the representations from the preceding and current layers, as illustrated in Figure 12. Building upon Equations 7 to 10, and contrasting with ScMoE, DGMoE can be formulated as

$$\begin{aligned} \mathcal{H}_{l+1}^{\text{DGMoE}} &= \mathcal{H}_{l+1}^{MH} + \sum_{i=1}^N (G(\mathcal{H}_{l+1}^{MH})_i E_i(\mathcal{H}_{l+1}^{MH})) \\ &\quad + G(\mathcal{H}_l^{MH})_i E_i(\mathcal{H}_l^{MH}) \end{aligned} \quad (19)$$

where $\mathcal{H}_{l+1}^{\text{DGMoE}}$ refers to the output from the MoE module.

However, as delineated in Equation 19, a potential issue arises when a token at the current layer selects the same top-1 expert as the preceding layer, inadvertently collapsing the intended top-2 gating mechanism into a de facto top-1 gating mechanism. To mitigate this, we introduce a constraint that ensures the activation of two distinct experts. In practice, this is achieved by first documenting the indices of experts triggered by the preceding-layer representations. Subsequently, if the preceding-layer representation coincidentally targets the same expert as the current layer, that is, $\overline{\text{Top}K}(H(\mathcal{H}_l^{MH}), 1) = \overline{\text{Top}K}(H(\mathcal{H}_{l+1}^{MH}), 1)$, we activate the second-highest-ranking expert from the top-2 selection for the current layer, i.e., $\overline{\text{Top}K}(H(\mathcal{H}_{l+1}^{MH}), 2)_2$.

As illustrated in Table 6 and Table 7, our DGMoE achieves comparable accuracy to the standard top-2 MoE across both vision and language tasks. Meanwhile, our ScMoE demonstrates performance more akin to the shared-expert MoE.

Table 5. Comparison of top-1 accuracy on the ImageNet-1K test set for SwinV2-MoE-S models, with and without the shared-expert gate (denoted as “SE-Gate”).

Model	With SE-Gate	Without SE-Gate
Our ScMoE (Pos-1)	79.14%	78.78%
Our ScMoE (Pos-2)	79.38%	78.98%
Our ScMoE (Pos-3)	79.20%	78.29%
Shared-Expert MoE	79.53%	79.02%

Table 6. Comparison of top-1 accuracy on the ImageNet-1K test set for SwinV2-MoE-S and SwinV2-MoE-B models with various architectures: top-2/top-1 gating standard MoE, shared-expert MoE, our DGMoE, and ScMoE, each pre-trained for 90 epochs on the ImageNet-1K classification dataset.

Model	SwinV2-MoE-S (Acc@1↑)	SwinV2-MoE-B (Acc@1↑)
Standard top-2 MoE	79.33%	80.48%
Standard top-1 MoE	78.95%	80.05%
Shared-Expert MoE	79.53%	80.62%
Our DGMoE	79.35%	80.51%
Our ScMoE	79.38%	80.56%

A.3 Analysis of Shared Expert Gate

In contrast to the gate-selected expert, the shared expert is fixed to process all representations without computing a gating score through the gating network. Therefore, common practices for shared-expert MoE employ a shared-expert gate to generate the coefficient for the shared expert’s output (Team, 2024; Dai et al., 2024). Specifically, the shared-expert gate is a linear layer that uses the input representation of the MoE module as its input to generate a coefficient similar to a gating score. Building upon Equation 6, the output of the shared expert can be expressed as

$$SE(x) = SEGate(x) \cdot MLP(x) \quad (20)$$

where $SEGate(\cdot)$ denotes the shared-expert gate and $MLP(\cdot)$ represents the essence of the shared expert.

As demonstrated in Table 5, the incorporation of the shared-expert gate significantly enhances model performance in our experimental vision tasks. In the absence of the shared-expert gate, the quality of MoE architectures with shared experts declines from that of a standard top-2 MoE to that of a standard top-1 MoE, despite maintaining the same computational volume as the standard top-2 MoE.

A.4 Evaluation Across Different Model Sizes

Table 6 and Table 7 illustrate that our experimental MoE architectures consistently achieve analogous model quality across different model sizes, as expounded in the detailed analysis within the main body of this paper.

Table 7. Comparison of zero-shot perplexity on WikiText-103 for our pre-trained GPT2-MoE-Small and GPT2-MoE-Medium models with various architectures.

Model	GPT2-MoE-Small (Perplexity↓)	GPT2-MoE-Medium (Perplexity↓)
Standard top-2 MoE	31.60	19.18
Shared-Expert MoE	29.15	17.94
Our DGMoE	31.52	18.91
Our ScMoE	29.10	17.62

A.5 Share MoE Across Multiple Layers via Shortcut Connections

From a certain point of view, our shortcut-connected MoE architectures can be conceptualized as the sharing of one MoE module across multiple transformer layers. Parameter sharing across different layers has been validated as a method to enhance parameter efficiency and improve model quality, as evidenced in existing research (Lan et al., 2019; Dehghani et al., 2018; Xue et al., 2022; Huang et al., 2017).

The empirical analysis of our novel MoE architectures suggests that the MoE modules shared across multiple layers via shortcuts could offer a more parameter-efficient solution. We conduct experiments on a preliminary architecture DGMoE-Share which shares a single MoE for two pairs of transformer blocks. It reduces the parameter count from 157M to 124M, while maintaining the same volume of expert computation as the standard top-1 MoE. The DGMoE-Share achieves a 78.45% accuracy on the vision task, incurring a minimal accuracy decrement of 0.5% relative to the standard top-1 MoE. We anticipate the discovery of more efficient architectures through future explorations. Additionally, the optimization of training hyperparameters for the shortcut-connected MoE requires more investigation.

A.6 Experimental Details

Table 8 summarizes the hyperparameters for training the GPT-MoE models including GPT2-MoE-Small, GPT2-MoE-Medium and GPT3-MoE-XL. We implement our models based on the Fairseq (Ott et al., 2019) and Tutel (Hwang et al., 2022) frameworks. And we use the Openwebtext dataset (Gokaslan & Cohen, 2019) for pre-training, with the GPT-2 BPE tokenizer (Radford et al., 2019). In addition to evaluating the training curve, we also conduct a zero-shot evaluation on WikiText-103 (Merity et al., 2016) dataset. Additionally, we maintained uniform hyperparameters across all models to ensure comparability, and we recognize that optimal parameter tuning may further enhance model performance, a subject for subsequent research.

Table 9 summarizes the hyperparameters for training the

Table 8. Hyperparameters for GPT-MoE models.

Parameter	GPT2-MoE-Small	GPT2-MoE-Medium	GPT3-MoE-XL
Num. layers	12	24	24
Embedding dim	768	1024	2048
Num. attention heads	12	16	32
Num. experts per layer	8	8	8
Num. parameters	323M	1.1B	4.1B
Context/sequence length	1K	2K	2K
Training tokens	180B	180B	18B
Warmup tokens	100M	100M	10M
Batch size	256	64	32
Learning rate	1.0e-4	1.0e-4	1.0e-4
LR-Scheduler	Inverse_sqrt	Inverse_sqrt	Inverse_sqrt
Capacity factor	2.00	2.00	2.00
MoE loss coefficient	0.01	0.01	0.01

Table 9. Hyperparameters for SwinV2-MoE models.

Parameter	SwinV2-MoE-S	SwinV2-MoE-B
Image size	192×192	192×192
Window size	12×12	12×12
Embedding dim	96	128
Num. layers	[2, 2, 18, 2]	[2, 2, 18, 2]
Num. attention heads	[3, 6, 12, 24]	[4, 8, 16, 32]
Num. experts per layer	8/16	8
Batch size	1024	1024
Epochs	90	90
Warmup epochs	10	10
Base LR	1.25e-4	1.25e-4
Warmup LR	1.25e-7	1.25e-7
Min LR	1.25e-6	1.25e-6
Capacity factor	1.25	1.25
MoE loss coefficient	0.01	0.01

Swin-MoE models including SwinV2-MoE-S and SwinV2-MoE-B. We develop our experiments based on the models and MoE framework which are provided by Tutel (Hwang et al., 2022), and also follow its hyperparameter configurations. The number of gate-selected experts per MoE module corresponds to the number of GPUs. Specifically, the experiments related to overhead and acceleration analysis in a 2-node (16×A800-NVLink) scenario utilize 16 experts per MoE module, while other cases use 8 experts. Then, we pre-train the models on ImageNet-1K image classification dataset. To maintain the comparability of our experiments, we limit our modifications solely to the MoE architectures and keep the hyperparameters and random seeds consistent. In addition, the experimental results related to efficiency are the averages of multiple samples over different periods.